PAPER

Evaluation of Pt, Ni, and Ni–Mo electrocatalysts for hydrogen evolution on crystalline Si electrodes†

James R. McKone, Emily L. Warren, Matthew J. Bierman, Shannon W. Boettcher,‡ Bruce S. Brunschwig, Nathan S. Lewis* and Harry B. Gray*

The dark electrocatalytic and light photocathodic hydrogen evolution properties of Ni, Ni–Mo alloys, and Pt on Si electrodes have been measured, to assess the viability of earth-abundant electrocatalysts for integrated, semiconductor coupled fuel formation. In the dark, the activities of these catalysts deposited on degenerately doped p+-Si electrodes increased in the order Ni < Ni–Mo ≤ Pt. Ni–Mo deposited on degenerately doped Si microwires exhibited activity that was very similar to that of Pt deposited by metal evaporation on planar Si electrodes. Under 100 mW cm^{-2} of Air Mass 1.5 solar simulation, the energy conversion efficiencies of p-type Si/catalyst photoelectrodes ranged from 0.2–1%, and increased in the order Ni ≈ Ni–Mo < Pt, due to somewhat lower photovoltages and photocurrents for p-Si/Ni–Mo relative to p-Si/Ni and p-Si/Pt photoelectrodes. Deposition of the catalysts onto microwire arrays resulted in higher apparent catalytic activities and similar photoelectrode efficiencies than were observed on planar p-Si photocathodes, despite lower light absorption by p-Si in the microwire structures.

I. Introduction

An approach to artificial photosynthesis involves the use of semiconductors to capture and convert sunlight into charge-separated electrons and holes. The separated charge carriers would then be coupled to suitable electrocatalysts to facilitate multi-electron transfer processes that effect, at low over-potentials, the oxidation of water to $O_2(g)$ and the reduction of water to $H_2(g)$.[1,2] Semiconductor photocathodes have shown high efficiency for production of $H_2(g)$ from H_2O, with nearly unity internal quantum yields throughout the visible region of

Beckman Institute and Kavli Nanoscience Institute, Division of Chemistry and Chemical Engineering, California Institute of Technology, 1200 East California Blvd, Pasadena, California, 91125, USA. E-mail: nslewis@caltech.edu; hbgray@caltech.edu
† Electronic supplementary information (ESI) available. See DOI: 10.1039/c1ee01488a
‡ Current address: Department of Chemistry, University of Oregon, Eugene OR.

the solar spectrum.[3] For example, p-InP/Rh photocathodes have yielded 11% thermodynamically based energy conversion efficiencies of HCl(aq) to $H_2(g)$.[4] Additionally, p-type Si photocathodes with an overlayer of Pt nanoparticles have been shown to produce >5% thermodynamically based conversion efficiency of protons to $H_2(g)$ under low-level monochromatic (632 nm) light in mildly acidic aqueous solution.[5] Several devices that have incorporated multi-junction semiconductor photoelectrodes have effected the overall solar-driven splitting of water to $H_2(g)$ and $O_2(g)$ with >5% efficiency.[6,7]

A globally scalable system for production of $H_2(g)$ from sunlight and H_2O will require light absorbers and electrocatalysts that are made from earth-abundant materials. In this respect, photocathodes formed from Si microwire arrays are attractive. The microwire array geometry orthogonalizes the directions of light absorption and charge-carrier collection, thereby facilitating the use of materials that have relatively low minority-carrier collection lengths.[8] Such materials, in turn, can be grown

Broader context

The development of carbon-neutral energy supplies is a critical goal for the 21st century. Solar energy is a massive resource, but to enable its use upon demand, storage methods, especially in the form of chemical fuels, are needed. Catalysts are required to convert with low energy loss the uncorrelated electron–hole pairs produced by captured sunlight into processes that make and break chemical bonds. Most such catalysts, however, contain rare and expensive second- or third-row transition metals. In this work, we have demonstrated the advantageous use of structured, high internal surface area microwire array semiconducting electrodes to obtain performance from abundant metal catalysts such as Ni or Ni–Mo that is sufficient to convert water into $H_2(g)$ with small energy loss at a rate comparable to the unconcentrated solar flux.

This journal is © The Royal Society of Chemistry 2011

Energy Environ. Sci., 2011, **4**, 3573–3583 | 3573

using high growth rate methods such as the vapor-liquid-solid growth technique.[9,10] Exploitation of the orthogonalization approach has to date yielded Si microwire array-based radial n[+]-p junction photovoltaic devices that, while only absorbing 60% of the light, have resulted in 7% solar energy conversion efficiencies under simulated Air Mass (AM) 1.5 illumination conditions.[11] Radial n[+]-p junction Si microwire array photocathodes that have been decorated with islands of Pt as an electrocatalyst have yielded, with only ~50% light absorption, >5% thermodynamically based energy conversion efficiencies for the production of $H_2(g)$ from 0.5 M H_2SO_4(aq) under simulated AM1.5 illumination.[12] A goal is therefore to use earth-abundant electrocatalysts to achieve performance for $H_2(g)$ evolution that is comparable to that obtainable using Pt or Pd as electrocatalysts.

The use of microwire arrays, or other electrodes that have a high ratio of their internal surface area to their projected, geometric area (i.e. a large roughness factor, γ) relaxes the constraints on catalyst activity needed to produce, at low overpotentials, fuels from sunlight. In an optimally operating tandem light absorbing structure under 1 Sun of AM 1.5 illumination, the solar photon flux will produce a charge-carrier flux of ~10–20 mA cm^{-2} to a planar electrode surface. This flux dictates the electrocatalytic activity necessary under unconcentrated AM1.5 sunlight for an efficient sunlight-driven water splitting system. Materials that have high γ values should relax this constraint on the needed catalytic activity, because the photogenerated charge-carrier flux can be distributed over a high internal surface area (Fig. 1). Hence for photoelectrodes with a high γ value, a lower inherent electrocatalytic activity is required to support the photogenerated charge-carrier flux relative to that needed to produce efficient planar photoelectrode. Stated differently, electrodes with high γ values provide an increased number of catalytic centers, and therefore lower the turnover frequency required of each catalyst unit.

The goal of this work is to identify earth abundant materials that could provide sufficient electrocatalytic performance to

support the low overpotential production of $H_2(g)$ on Si photocathode surfaces under solar illumination. One approach is to enhance the low electrocatalytic activity of abundant materials by exploiting the large γ values obtainable for Si microwire array structures and related photoelectrode morphologies. Ni and Ni–Mo are known electrocatalysts for $H_2(g)$ production,[13–19] and in smooth forms ($\gamma \approx 1$) have exhibited exchange current densities between 10^{-6} and 10^{-4} A cm^{-2} in acidic electrolyte, compared to 10^{-3} A cm^{-2} for Pt.[14,19] Although Ni or Ni–Mo would provide inferior performance at high current densities compared to Pt, e.g. in proton-exchange membrane (PEM) based electrolyzers, which must minimize the area-related capital expenses associated with the membrane-electrode assembly and the balance of systems in such devices, such electrocatalysts might be viable alternatives to Pt, when deposited onto Si microwire array photocathode surfaces.

Accordingly, we have investigated the behavior of Ni and Ni–Mo alloy electrodeposited from weakly acidic solutions onto planar and microwire array Si substrates, respectively, of either degenerate (p[+]) or p-type doping. The electrochemical and photoelectrochemical hydrogen evolution reaction (HER) activities of these composite electrodes have been compared to each other as well as to that of two types of Si/Pt electrodes. The photoelectrode behavior of such systems has been correlated with the catalyst composition and morphology, and with the known characteristics of p-Si photocathodes and Si microwire arrays, to assess the viability of this class of non-noble catalysts for use in photoelectrochemical $H_2(g)$ production systems.

II. Experimental

A. Fabrication of electrodes

Si wafers of (100) orientation and p-type doping with resistivities, ρ, of ~0.7 Ω cm (p-Si), were obtained from Silicon Inc. Degenerately doped p-type, (111)-oriented Si wafers with ρ <0.001 Ω cm (p[+]-Si) were obtained from Silicon Quest International. Si microwire arrays were grown on p[+]-Si substrates by an atmospheric pressure chemical vapor deposition (CVD) technique that used Cu as a vapor-liquid-solid (VLS) growth catalyst.[9] The hexagonal wire pattern was determined by the pattern of the Cu, which was defined by evaporation and lift-off of Cu into lithographically etched holes in a SiO_2 buffer layer on the Si substrate. For wire growth, $SiCl_4$(g) was the Si source and BCl_3(g) was the boron source, resulting in p-type doping of the crystalline Si microwires. After growth, the microwire arrays were etched to remove the Cu growth catalyst from the wire surfaces (see ESI†).

Planar p[+]-Si electrodes, and all Si microwire array electrodes, were fabricated by a multistep procedure in which the wafer/array was first scribed and cut into pieces that were ~5 mm on a side. An ohmic back contact was then formed by use of a diamond scribe to scratch a Ga/In eutectic mixture (Aldrich) onto the unpolished back sides of the pieces. The pieces were then affixed to tinned copper wire using silver paint (SPI, Inc.), and allowed to dry overnight. The resulting electrode assembly was sealed onto a glass capillary using a 2-part epoxy (Hysol 1C; chosen for chemical stability). The final electrode area was defined using Hysol 9460 epoxy (chosen for dark color and high
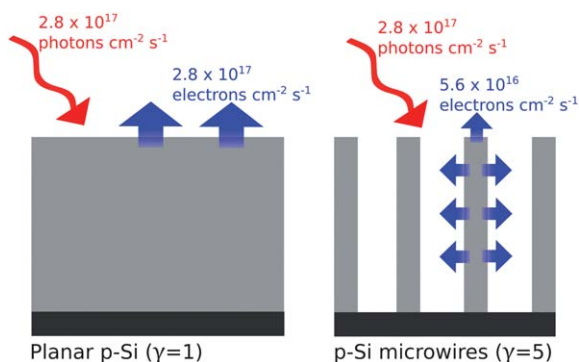

Fig. 1 Relationship between the incident photon flux and outgoing electron flux in a conventional crystalline Si absorber (left), and a crystalline Si microwire array (right) under AM1.5 illumination, assuming unity absorption above the Si bandgap and unity quantum yield for charge carrier collection. The microwire array produces a smaller electron flux per absorber surface area, even for the same incident photon flux, due to the roughness factor of $\gamma = 5$ that results from its microstructured geometry.

viscosity before curing). Planar p-Si electrodes were fabricated according to the same process, except that the back, ohmic contact was provided by sputter-deposition of ∼500 nm of Al, followed by heating the sample for 10 min at 450 °C under vacuum. Immediately prior to use, all of the Si electrodes were etched in aqueous NH_4F/HF (buffered HF, Transene) until the surfaces were hydrophobic, indicating the removal of surface Si oxides and the formation of surface Si hydrides.

B. Deposition of electrocatalysts

1. Deposition of Ni or Ni–Mo. Ni was electrodeposited from a sulfamate solution that consisted of 325 g L^{-1} Ni(II) sulfamate and 30 g L^{-1} H_3BO_3, with the pH adjusted to ∼4.0 using KOH.[20] For deposition of Ni–Mo, 5 g L^{-1} Na_2MoO_4 were added to the above solution before final adjustment of the pH.

Electrodeposition was carried out either galvanostatically or potentiostatically, using a Gamry Reference 600 potentiostat/galvanostat. Depositions were performed in air, in a one–compartment cell, using a large area Ni counter electrode and a Ag/AgCl (1 M KCl, $E^{\circ\prime} = + 0.222$ V *vs.* the normal hydrogen electrode, NHE) reference electrode.

Ni was deposited for 0.5–5 s onto planar Si electrodes by application of a bias sufficient to produce a cathodic current density of 20 mA cm^{-2}, resulting in passage of 10–100 mC cm^{-2} of cathodic charge density. Ni–Mo deposition onto planar Si electrodes was performed for 5–180 s at a cathodic current density of 20 mA cm^{-2}, producing 100–3600 mC cm^{-2} of cathodic charge density. Electrocatalyst deposition on Si microwire array electrodes was performed galvanostatically at 50 mA cm^{-2} of cathodic current density, or was performed potentiostatically at a potential that produced ∼20 mA cm^{-2} of cathodic current density on the corresponding planar Si electrode surface. The range of total deposition times tested for Si microwire array electrodes was somewhat longer than for planar Si electrodes.

All p^+-Si electrodes were sufficiently conductive that they behaved like metals in the plating solution. In contrast, the p-Si photoelectrodes exhibited carrier depletion in the plating solution, which generated a barrier to cathodic current flow in the dark. These electrodes were therefore illuminated using an ELH-type tungsten-halogen light source that was placed immediately adjacent to the cell that contained the plating solution. The Si microwire electrodes were tilted at a slight angle relative to the incident light propogation vector, thereby providing sufficient absorbed photon flux to effect facile transfer of photogenerated charge carriers across the interface and thus enable photo-deposition of the electrocatalyst.

The conditions and time intervals for electrocatalyst deposition produced a range of catalyst loadings on the Si surface, as observed by scanning electron microscopy (SEM). In some cases, the electrocatalysts were deposited in several stages, with HER testing between each stage, to observe increases or decreases in the catalytic activity as a function of increases in catalyst loading. The non-noble catalyst coatings were stable over the several hour timescale of photoelectrochemical measurements.

2. Deposition of Pt. Pt was deposited onto planar or microwire Si electrodes by electroless deposition or by electron beam (e-beam) evaporation. The electroless deposition of Pt was performed by placing a drop of 1 mM K_2PtCl_6(aq) in 0.5 M HF (aq) on the electrode surface for 2 min, followed by a thorough rinse with >18 MΩ resistivity H_2O. The HER performance of the electrode was then evaluated, and the process was repeated until the HER activity, as measured by the cathodic current density passed at a given potential (vide infra), reached a plateau or started to decrease. Generally the highest catalytic activity was observed after a total time of 4–6 min of plating. E-beam evaporation of Pt was performed under a vacuum of <10^{-5} torr in a Denton Explorer evaporator system. Approximately 1 nm of Pt was evaporated onto a completely assembled electrode, at a deposition rate of 0.1–1 Å s^{-1}.

C. Characterization of deposited electrocatalysts

Structural characterization of the various electrocatalyst deposits on Si electrodes was performed using a Zeiss model 1550 field-effect scanning electron microscope. To prepare samples for characterization by SEM, the glass tube in which the sample had been mounted was scribed and broken, to expose a length of bare Cu wire. The sample was then fixed to the sample stage, and to minimize charging effects, the bare Cu wire was electrically grounded to the stage. Electron micrographs were collected promptly after the current-potential behavior of the electrodes had been determined with regard to H_2(g) evolution.

Further structural characterization was performed using an FEI TF30UT transmission electron microscope (TEM) that was equipped with a HAADF STEM detector, an Oxford energy-dispersive X-ray detector, and a high-resolution CCD camera. For TEM analysis, a layer of catalyst was deposited onto a Si electrode and was subsequently scraped off with a stainless steel razor blade. The resulting powder was suspended in isopropanol and then drop cast onto a lacey carbon/Cu grid. Compositional and crystal phase data were collected using energy-dispersive X-ray spectroscopy (EDS) and electron diffraction, respectively. The SEM and TEM images were subjected to a minimum of post-processing, being limited to normalization of the white-balance to a level that produced optimal contrast in the images.

X-ray photoelectron spectroscopic (XPS) analysis was carried out using a Kratos Ultra DLD instrument that was equipped with a magnetic immersion lens with a spherical mirror and concentric hemispherical analyzers. All XP spectra were fit using a software package that was written in-house and minimized the χ^2 fitting error with the Levenberg–Marquardt algorithm. Spectra were fit with Gaussian–Lorentzian line shapes above a Shirley background with no asymmetric profiles.

D. Electrochemical measurements

The activities of the various catalysts and the performance of photoelectrodes were measured using a Gamry Reference 600 potentiostat/galvanostat. Electrodes were evaluated in aqueous 0.2 M potassium hydrogen phthalate (KHP) with 0.5 M K_2SO_4 supporting electrolyte, buffered to pH 4.5 using KOH. This electrolyte acted as a stable pH buffer, produced a stable reversible hydrogen electrode (RHE) potential, and represented the best compromise between activity and stability for all of the systems tested in this work.

Electrochemical experiments were performed in a two-compartment Pyrex cell equipped with a flat Pyrex window and with a saturated calomel electrode (SCE) reference ($E^{\circ\prime}$ = +0.244 V vs. NHE, CH Instruments). A Pt mesh counter electrode was contained in a separate compartment that was isolated from the main cell compartment by a fine porosity frit. All of the electrochemical data were collected with fast stirring of the solution, to minimize mass transport effects and rapidly remove nucleated bubbles from the electrode surface.

The electrolyte was constantly bubbled with research grade $H_2(g)$ (AirLiquide) to maintain a constant RHE potential, as determined by measurement of the open-circuit potential of a platinized Pt wire before and after each set of measurements. The RHE potential was consistently measured to be -505 ± 5 mV vs. SCE, in close agreement with the value predicted by the Nernst equation at pH 4.5. The measured RHE potential did not shift by more than ± 1 mV over the course of several hours of measurements.

Electrodes were tested using cyclic voltammetry (CV) or linear sweep voltammetry (LSV), both at a scan rate of 20 mV s^{-1}. The current density versus potential (J–E) data were not corrected for any uncompensated resistance losses or for concentration overpotentials. In the case of CV, forward and reverse sweeps generally showed minimal hysteresis. Where hysteresis was observed, the data collected while sweeping from negative toward positive potentials (reverse sweep) were found to correspond better to steady-state polarization measurements, and thus were used for final analysis. LSV measurements generally began at a potential 300–800 mV negative of RHE, and ended just positive of where the electrode began to pass anodic current. The potential limits for cyclic voltammetry were set to prevent the passage of large anodic current densities. These precautions were taken to prevent the Si surface from oxidizing and to minimize anodic stripping of the non-noble catalyst particles from the electrode surface.

The photoelectrode performance was evaluated under simulated sunlight supplied by a home-built ELH-type tungsten-halogen light source. The light source was placed at a distance from the electrochemical cell sufficient to generate an incoming photon flux equivalent to 1 Sun illumination, as measured by a Si photodiode (Thorlabs) that was calibrated relative to a NIST-traceable standard (Solarex).

III. Results

A. Composition and morphology of the deposited electrocatalysts

1. SEM data for Ni, Ni–Mo and Pt electrocatalysts deposited onto planar Si electrodes. All three of the materials deposited on planar Si electrodes as nanoparticles, as indicated by SEM data (Fig. 2). The Ni particles nucleated and rapidly grew to ~100 nm in diameter, and coalesced into a continuous film as the deposition time increased from 0.5 to 5 s. Electrodeposition of Ni–Mo produced somewhat smaller nanoparticles and smaller interparticle distances than were observed for electrodeposited Ni. When the deposition time for the Ni–Mo films was increased from a few seconds to several minutes, the particles did not coalesce into a continuous layer, but instead formed multilayers composed of progressively larger agglomerates of particles. These multilayers remained porous, as underlying layers of the electrodeposited Ni–Mo film were visible in the SEM.

In contrast, the electroless deposition of Pt produced a discontinuous nanoparticulate film.[21] Increases in the deposition time, from 2 to 8 min, increased the density of Pt nanoparticles, eventually creating large island-like agglomerates that began to flake off of the Si surface. Deposition of Pt by electron beam evaporation, even of a nominally ~1 nm thick coating, gave a film that was difficult to image clearly by SEM, but resulted in enhanced catalytic activity for the HER that was consistent with the deposition of Pt (vide infra).

2. TEM data for electrocatalysts deposited onto planar p-type Si electrodes. TEM analysis of the Ni–Mo (Fig. 3) and Ni (see ESI†) films indicated that the mean crystallite sizes in the deposits were ~5 ± 2 and ~10 ± 5 nm (1σ), respectively. Electron diffraction and EDS indicated that the Ni–Mo film was single phase, with a lattice spacing that closely matched the Ni face-centered-cubic lattice, and with a bulk composition of ~85% Ni/~15% Mo.

3. SEM data for electrocatalysts deposited onto Si microwire arrays. As probed by SEM, on p⁺-Si microwire arrays, Ni, Ni–Mo, and Pt produced homogeneous and conformal deposits over the entire surface of the microwires (Fig. 4). In contrast, on p-Si microwires, the deposits were only evident by SEM on the bottom halves of the wires, but EDS analysis indicated that catalyst had deposited over the entire wire surface.

B. Dark current-density vs. potential behavior of electrodeposited catalysts on degenerately doped planar Si electrodes

Representative polarization data for Ni, Ni–Mo, and Pt on planar p⁺-Si electrodes are depicted in Fig. 5 and are summarized in Table 1. The aggregate activities of the various catalyst materials were assessed quantitatively by comparing the cathodic current density observed at a HER overpotential of 100 mV ($J_{\text{dark},100}$).[22] This measure of activity included both the electronic and geometric (surface area) contributions to the hydrogen evolution activity of the various deposits.[23] Using this metric, the activities for the three catalyst systems on planar p⁺-Si electrodes increased in the order Ni < Ni–Mo ≤ Pt.

Ni consistently showed the most negative onset potential of appreciable cathodic current density, reaching only $J = -0.12$ mA cm^{-2} at $E = -100$ mV vs. RHE when Ni had been electrodeposited for 5 s on to the p⁺-Si surface. Shorter deposition times produced lower catalytic activity, and longer deposition times produced relatively smooth, continuous Ni films that had similar activities to the Ni data shown in Fig. 5. The J–E behavior observed herein for Ni on Si is very close to the behavior observed previously for the HER of Ni-plated Fe electrodes.[24]

Ni–Mo alloy films on planar p⁺-Si gave J–E responses that exhibited increasing catalytic activities over several min of deposition. Deposition for 20–30 s produced films with a single layer (as observed by SEM) of Ni–Mo deposit, and produced ~2 mA cm^{-2} of cathodic current density for the HER at
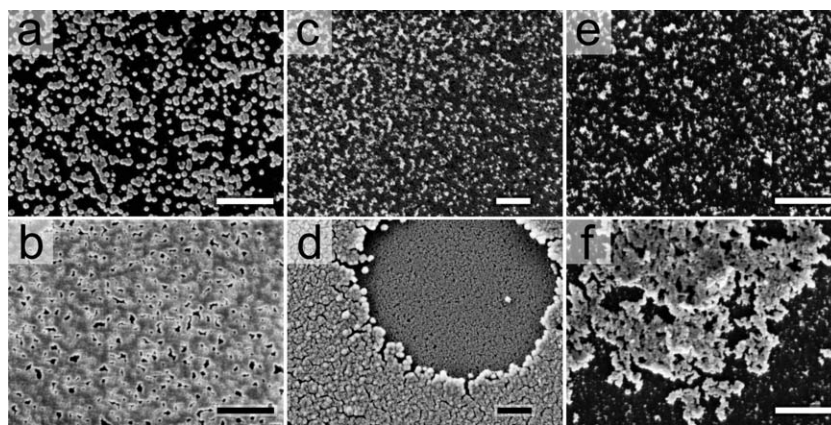
Fig. 2 Scanning electron micrographs of catalyst particles on planar Si surfaces: (a) Ni deposited for 0.5 s; (b) Ni deposited for 1.0 s; (c) Ni–Mo deposited for 30 s; (d) Ni–Mo deposited for 90 s; (e) electroless Pt deposited for 360 s (f) same as e, but showing a Pt agglomerate. The scale bar in each panel is 1 μm.
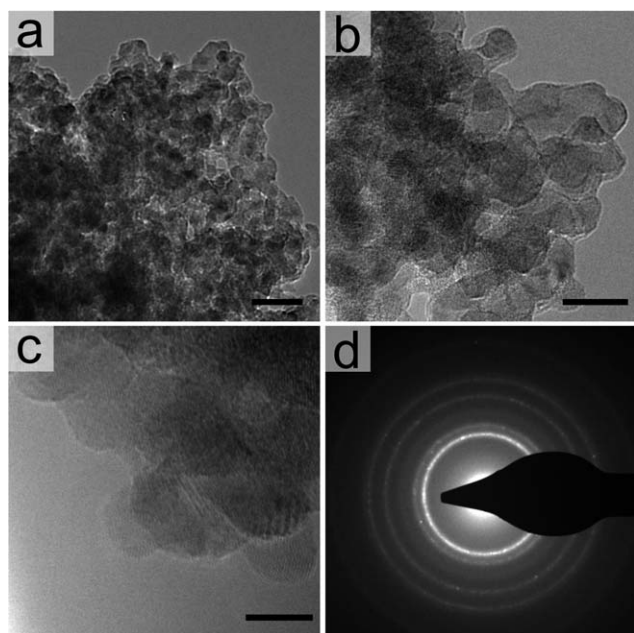

Fig. 3 (a–c) TEM images and (d) electron diffraction pattern of a Ni–Mo film that was electrodeposited onto a p$^+$-Si electrode. The images indicate that the Ni–Mo deposits were agglomerates of <10 nm crystallites. Scale bars: (a) 20 nm; (b) 10 nm; (c) 5 nm.

$E = -100$ mV *vs.* RHE. Deposition for >30 s produced films that had a multilayer structure and yielded HER cathodic current densities of >5 mA cm^{-2} at $E = -100$ mV *vs.* RHE.

The two techniques used to deposit the Pt electrocatalyst yielded different *J*–*E* responses on planar p$^+$-Si electrodes. The onset of cathodic current obtained for the electroless deposition of a Pt electrocatalyst deposit was similar to that observed for Ni–Mo that had been deposited on p$^+$-Si for 90 s, giving nearly -5 mA cm^{-2} at $E = -100$ mV *vs.* RHE. As the potential was scanned more negative relative to RHE, the electroless Pt films produced a very linear *J*–*E* electrocatalytic response, indicating resistive behavior. In contrast, Pt films that had been deposited by electron-beam evaporation, although nominally only ∼1 nm

thick, were highly active electrocatalysts on p$^+$-Si for the HER, reaching $J = -20$–30 mA cm^{-2} at $E = -100$ mV *vs.* RHE. Furthermore, at higher cathodic current densities, the e-beam deposited Pt films showed the expected exponential response rather than the linear response that was observed for electroless Pt deposits on p$^+$-Si.

C. Dark current-density *vs.* potential behavior of electrodeposited catalysts on degenerately doped Si microwire array electrodes

The catalytic activities of Ni, Ni–Mo, and Pt, respectively, were considerably higher, but exhibited the same trend in relative activity, on p$^+$-Si microwire arrays relative to the activity on planar p$^+$-Si electrode surfaces (Fig. 6, Table 1). The *J*–*E* response of electroless Pt deposits was closer to that of e-beam Pt deposits on p$^+$-Si microwires than on the planar p$^+$-Si electrodes, but the *J*–*E* response was still relatively linear at large cathodic current densities.

Fast stirring and continuous bubbling of H$_2$(g) through the solution were required to obtain reproducible *J*–*E* responses for planar and microwire array p$^+$-Si electrodes. The *J*–*E* data generally proceeded cleanly through $J = 0$ at $E = 0$ *vs.* RHE under these conditions, but only using the LSV technique, beginning at negative potentials and proceeding in the positive direction. An exception was the case of Ni–Mo alloy electrodeposited onto p$^+$-Si microwires, which often passed through $J = 0$ at $E < 0$ *vs.* RHE, similar to the behavior observed previously with bulk Ni–Mo alloy cathodes as well as with electrodeposited Ni–Mo–Cd films.[24]

D. Photoelectrochemical behavior of electrocatalysts on p-Si electrodes

Six metrics were used to evaluate the photoelectrochemical performance of Ni, Ni–Mo, and Pt, respectively, as electrocatalysts on illuminated planar p-Si or p-Si microwire array photocathodes in contact with pH = 4.5 aqueous solutions (Fig. 7, 8, Table 2). These metrics [eqn (1) to (6)] were:

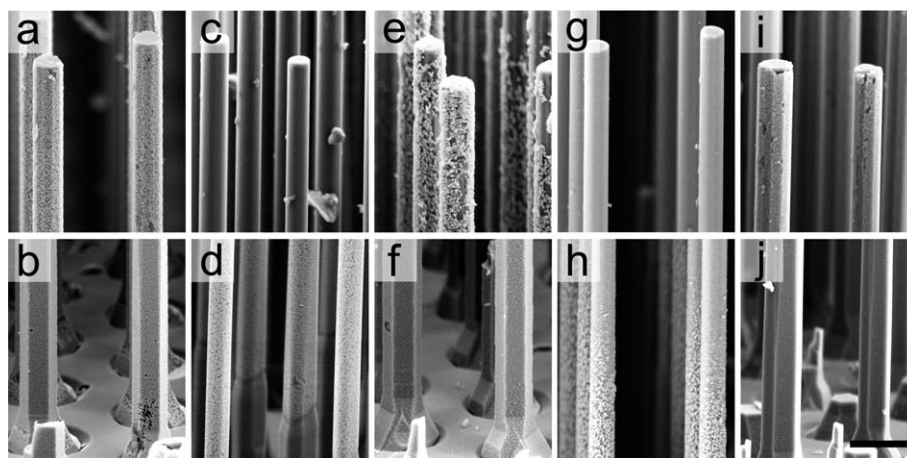$$V_{oc} = |E_{oc} - E_{RHE}| \tag{1}$$

Fig. 4 Scanning electron micrographs of catalyst particles on Si microwire tops (above) and bases (below): (a, b) p+-Si deposited with Ni for 5 s; (c, d) p-Si deposited with Ni for 1 s; (e, f) p+-Si deposited with Ni–Mo for 90 s; (g, h) p-Si deposited with Ni–Mo for 20 s; (i, j) p+-Si deposited with electroless Pt for 360 s. The scale bar in (j) is 3 μm, and applies to all panels.
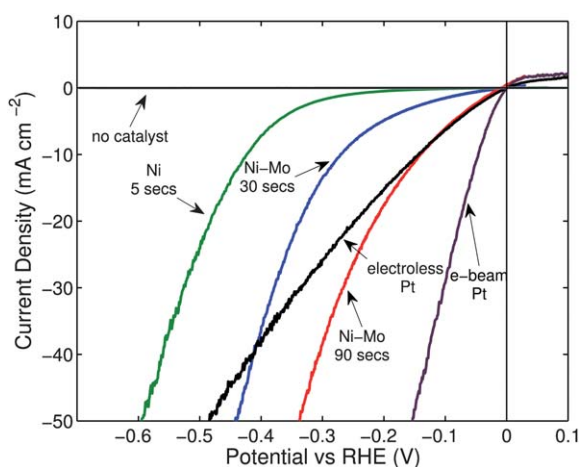

Fig. 5 Polarization data of the HER activities of various catalysts on planar p+-Si electrodes. The total deposition times for electrodeposited catalyst films are specified. Data were collected at pH = 4.5, and are referenced to the RHE potential.

$$J_{light,100} = J|_{E_{oc} - 100 \text{ mV}} \quad (2)$$

$$J_{sc} = J|_{E_{RHE}} \quad (3)$$

$$J_{ph} = J|_{E_{RHE} - 0.4 \text{ V}} \quad (4)$$

$$ff = \frac{P_{max}}{V_{oc} \cdot |J_{sc}|} \quad (5)$$

$$\eta_{H_2} = \frac{P_{max}}{P_{in}} = \frac{ff \cdot V_{oc} \cdot |J_{sc}|}{P_{in}} \quad (6)$$

a) the open-circuit voltage (V_{oc}, eqn (1)), which indicates, relative to RHE, the maximum free energy that can be extracted from the photoelectrode, where E_{oc} is the potential at which the photo-electrode passed no current; b) the apparent aggregate catalytic activity ($J_{light,100}$, eqn (2)) measured as the current density passed at a potential 100 mV negative of E_{oc}; c) the short-circuit current density (J_{sc}, eqn (3)), the current density at $E = 0$ V vs. RHE; d)

the light-limited photocurrent density (J_{ph}, eqn (4)), measured as the current density at $E = -0.40$ V vs. RHE; e) the fill factor (ff, eqn (5)), a measure of the "squareness" of the J–E response, where P_{max} is the maximum product of $|J|$ and E; and f) the thermodynamic efficiency for production of $H_2(g)$ (η_{H_2}, eqn (6)), where P_{in} is the incoming light intensity, 100 mW cm^{-2} for AM 1.5 simulated sunlight.

1. Apparent catalytic activities. The apparent catalytic activities for p-Si photoelectrodes, both in planar and microwire array forms, followed the same order, Ni < Ni–Mo ≤ Pt, as was observed for these catalysts on un-illuminated p+-Si electrodes. In general, however, the photoelectrodes required a more negative potential (relative to E_{oc}) to produce a given current density than dark electrodes (relative to E_{RHE}) that had been deposited with the same catalyst material. The exception was Ni, which exhibited a somewhat more rapidly increasing onset of cathodic current density on illuminated p-Si photoelectrodes than on dark p+-Si electrodes, especially when Ni had been deposited onto p-Si microwire array photocathodes.

2. Open-circuit potentials. The V_{oc} values for the photo-cathodes followed the order Ni–Mo < Ni < Pt on both planar and microwire arrays of p-Si. Additionally, for electrodeposited Ni, the V_{oc} values were smaller by >100 mV on p-Si microwire arrays than on planar p-Si electrodes. Interestingly, the V_{oc} values obtained for Pt on p-Si photoelectrodes were dependent on the method of Pt deposition. Electron-beam evaporated Pt films yielded ohmic contacts to planar p-Si, resulting in high catalytic activity but no photovoltage, whereas electroless Pt deposition gave the largest photovoltages observed for any of the electrocatalytic deposits studied herein on both p-Si planar and microwire array electrodes.

3. Short-circuit photocurrent densities. The observed J_{sc} values for planar p-Si photoelectrodes generally were between −10 mA cm^{-2} and −25 mA cm^{-2}, depending on the length of time that the catalyst had been deposited. These J_{sc} values correspond to somewhat lower apparent quantum yields than have been

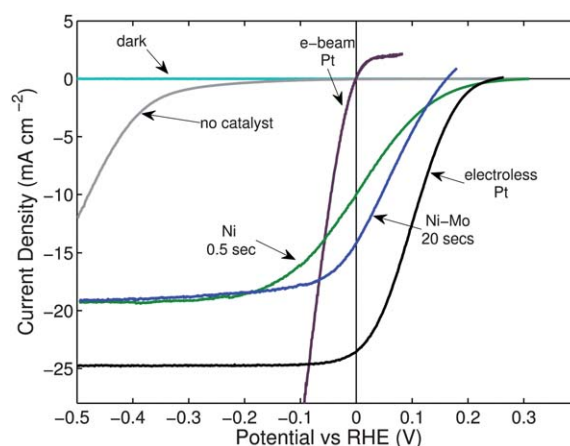**Table 1** Figures of merit for p[+]-Si dark electrocatalysis

Electrode	Geometry	Catalyst	Dep. time (s)	$-J_{dark,100}$ (mA cm^{-2})
15a	planar	none	0	0.01
42a	wires	none	0	0.02
14a	planar	Ni	0.5	0.05
17	planar	Ni	5	0.12
39c	wires	Ni	5	0.36
40a	wires	Ni	1	0.46
18a	planar	Ni–Mo	30	1.8
20b	planar	Ni–Mo	90	6.3
35a	wires	Ni–Mo	30	6.7
259-3	wires	Ni–Mo	60	10.4
38	wires	Ni–Mo	90	14.3
35c	wires	Ni–Mo	180	20.8
26a	planar	electroless Pt	120	0.8
26c	planar	electroless Pt	360	4.5
41a	wires	electroless Pt	120	1.4
42c	wires	electroless Pt	240	5.5
41c	wires	electroless Pt	360	12.2
23	planar	e-beam Pt	N/A	25.3
54	wires	e-beam Pt	N/A	35.0
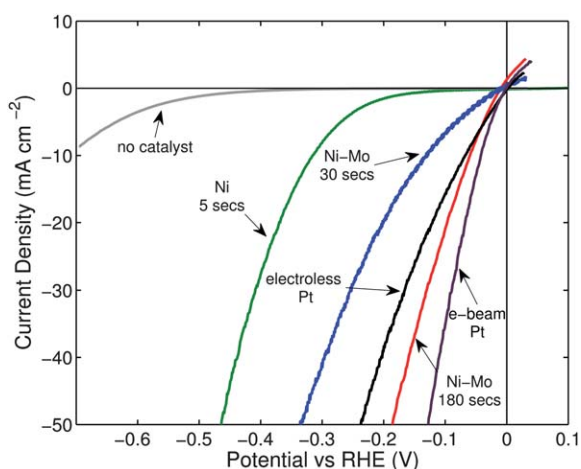
Fig. 6 Polarization data of the HER activities of various catalysts on p[+]-Si microwire electrodes. The total deposition times for electrodeposited catalyst films are specified. Data were collected at pH = 4.5, and are referenced to the RHE potential.

Fig. 7 Polarization data of the HER activities of various catalysts on illuminated planar p-Si photoelectrodes. The total deposition times for electrodeposited catalyst films are specified. Data were collected at pH = 4.5, and are referenced to the RHE potential.

observed for p-Si photoelectrodes under a controlled, monochromatic photon flux in contact with an aqueous methyl viologen (MV$^{2+/+}$) redox system,[25] indicating that the catalyst particles absorbed and/or reflected some of the incident light.

J_{sc} values for p-Si microwire array photoelectrodes were between −8 mA cm^{-2} and −15 mA cm^{-2} at normal incidence. These values increased in magnitude when the electrode was tilted by ∼35° relative to the propagation vector of the incident optical beam. These J_{sc} values are close to the values that have been reported for p-Si microwire arrays in contact with MV$^{2+/+}$(aq), as well as for HER using a Pt electrocatalyst, suggesting minimal net absorption or reflection by the catalyst particles.[12,25]

4. Overall photoelectrode performance. The thermodynamically based light-to-H$_2$ photoelectrode efficiencies ranged from ∼0.2% to ∼1%, and increased in the order Ni ≈ Ni–Mo < Pt. Because the higher V_{oc} values for Ni-decorated electrodes were

offset by higher catalytic activities for Ni–Mo, Ni and Ni–Mo coated Si photocathodes exhibited similar overall efficiencies of 0.2–0.4%. The fill factors for the Ni–Mo deposited photoelectrodes were somewhat higher than fill factors for electrodes that had Ni deposits, which is also consistent with the higher catalytic activity of Ni–Mo relative to Ni. P-type Si microwire array photoelectrodes gave overall thermodynamically based efficiencies for H$_2$ production that were similar to those of the corresponding planar p-Si electrodes, due to the generally lower photocurrent densities of the microwire arrays compensated by higher fill factors relative to the planar p-Si electrodes.

IV. Discussion

A. Deposition of the electrocatalysts

The Ni–Mo alloy deposition bath was based on an acidic Ni sulfamate plating bath,[20] rather than the widely used alkaline citrate or pyrophosphate baths.[26–28] The sulfamate solution
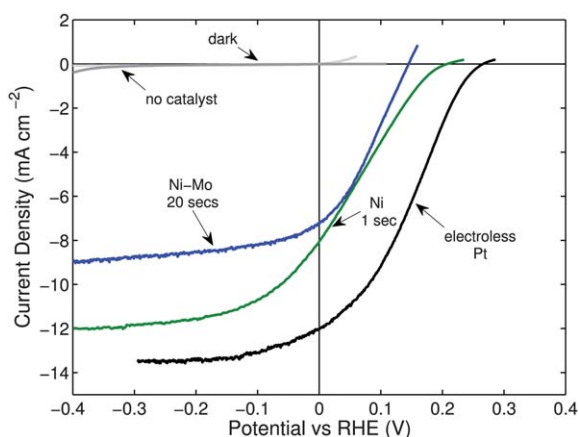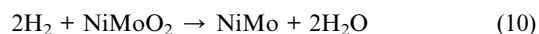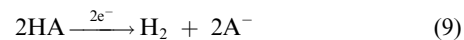
Fig. 8 Polarization data of the HER activities of various catalysts on illuminated p-Si microwire array photoelectrodes. The total deposition times for electrodeposited catalyst films are specified. Data were collected at pH = 4.5, and are referenced to the RHE potential.

avoided the instability of the Si surface toward oxidation under alkaline conditions. Use of alkaline Ni–Mo plating baths yielded inconsistent results, with the resulting deposits showing poor adhesion to the Si surface.

The Ni–Mo/sulfamate plating bath was similar to existing bath formulations, in that it involved the addition of Na_2MoO_4 to a Ni plating solution. However, the relative amount of Mo was much lower (~1.5 mol% Mo relative to total metal content) in the sulfamate bath compared to that contained in alkaline Ni–Mo deposition baths (>10% Mo).[26] Increases in the concentration of MoO_4^{2-} beyond 1.5% resulted in films that had poor adherence onto the Si electrode surfaces and also exhibited low activity for the HER. The Ni–Mo/sulfamate solution was stable over a period of months, with no evidence of changes in pH or formation of "molybdenum blue" precipitates.[29,30]

The formation of active Ni–Mo catalyst films required the use of relatively large cathodic deposition current densities (>10 mA cm^{-2}). At these current densities, bubbles were observed on the electrode surface, consistent with the simultaneous evolution of H_2 and deposition of Ni–Mo. The production of H_2(g) is consistent with a previously proposed deposition

mechanism in which evolved H_2(g) reduces the intermediate Ni–Mo mixed oxide to a neutral alloy [eqn (7) to (10)].[31]

$$MoO_4^{2-} + 4H^+ \xrightarrow{2e^-} MoO_2 + 2H_2O \quad (7)$$

$$Ni^{2+} + MoO_2 \xrightarrow{2e^-} NiMoO_2 \quad (8)$$

$$2HA \xrightarrow{2e^-} H_2 + 2A^- \quad (9)$$

$$2H_2 + NiMoO_2 \rightarrow NiMo + 2H_2O \quad (10)$$

Increases in the cathodic deposition current density, to 100 mA cm^{-2}, resulted in thick, gray-black deposits that exhibited poor HER activity, and that readily dissolved in acidic solution. The behavior at high deposition current densities is consistent with the precipitation of Ni hydroxides, due to the increase in local pH effected by the vigorous evolution of H_2(g) in the poorly buffered plating solution.

The relatively long times required to deposit single layers of Ni–Mo, compared to the deposition of Ni from the Ni/sulfamate bath, are also consistent with the co-evolution of H_2(g) during the deposition of Ni–Mo from the sulfamate solution. The deposition current efficiency of Ni–Mo from the sulfamate solution was <5%, as compared to nearly 100% under the noted conditions for Ni from the sulfamate solution (see ESI†). Consequently, the resulting films of Ni–Mo particles were generally discontinuous and contained micron-scale holes or inhomogeneities, likely due to H_2(g) bubbles blocking the surface from access to the plating solution.

B. Relative electrocatalytic activities

When polished to minimize variations in relative surface area, a Ni–Mo alloy has been shown to produce slightly higher fundamental HER activity than Ni,[19,24,32] but lower HER activity than bright (smooth) Pt.[33] Relative to smooth bulk Ni–Mo surfaces, enhanced HER activity has been documented for electrodeposited Ni–Mo, as evidenced by an increased exchange current density and a decreased Tafel slope, apparently due to micro/nanostructuring of the electrocatalytic deposits.[24]

Table 2 Figures of merit for photoelectrodes

Electrode	Geometry	Catalyst	Dep. time (s)	V_{oc} (mV)	$-J_{light, 100}$ (mA cm^{-2})	$-J_{sc}$ (mA cm^{-2})	$-J_{ph}$ (mA cm^{-2})	ff	η_{H_2} (%)
45a	planar	no catalyst	N/A	255	0.16	0.82	N/A	0.17	0.03
317-E0	wires	no catalyst	N/A	34	0.01	0.005	N/A	0.43	0
298-4	planar	Ni	0.5	340	0.28	10.0	19.0	0.11	0.4
298-8	planar	Ni	1	325	0.32	6.6	19.4	0.11	0.2
317-E1	wires	Ni	0.5	190	3.4	7.3	10.6	0.24	0.3
317-F2	wires	Ni	1	210	3.2	8.0	12.0	0.22	0.4
49	planar	Ni–Mo	20	140	7.9	11.6	15.6	0.22	0.4
46	planar	Ni–Mo	30	140	7.3	9.3	11.0	0.27	0.3
317D2	wires	Ni–Mo	20	145	5.7	6.8	8.3	0.33	0.3
317C2	wires	Ni–Mo	40	145	6.0	7.0	8.6	0.35	0.4
7c	planar	electroless Pt	180	245	2.4	16.8	19.0	0.17	0.7
9b	planar	electroless Pt	240	230	6.2	21.8	23.4	0.22	1.1
10c	planar	electroless Pt	360	240	2.4	18.1	25.6	0.16	0.7
10d	planar	electroless Pt	480	210	1.5	10.1	27.2	0.12	0.3
317G	wires	electroless Pt	120	265	5.0	11.7	13.1	0.31	1.0
12	planar	e-beam Pt	N/A	0	23.3	0	N/A	0	0

Notably, Ni–Mo coatings designed for maximum surface roughness have been reported to exhibit higher HER activities than smooth Pt, and are reported to be stable for >1 year in contact with alkaline electrolyte.[34,35]

When used as a catalyst on Si photoelectrodes, the maximum acceptable thickness (and hence roughness) of Ni–Mo is limited by the requirement of minimizing absorption of the incoming light. The observed order of catalyst activity on Si cathodes, Ni < Ni–Mo < Pt (provided that the Pt was not deposited by a method that gave rise to resistive behavior), is thus in accord with expectations. For all of the catalysts deposited on electrodes of nominally the same projected area, the HER activities observed on a Si microwire array exceeded those on planar Si electrodes, consistent with the increased amount of catalyst per projected surface area on the microwire arrays relative to compact, planar electrode surfaces.
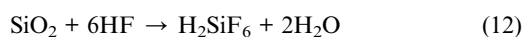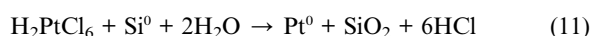
C. Degenerately doped dark Si electrode/catalyst systems

Relatively short electrodeposition times were required to reach maximum HER activity of Ni on p⁺-Si, owing in part to the high deposition current efficiency of Ni on Si. Deposition times < 1 s produced a discontinuous network of Ni particles, whereas longer times caused the Ni particles to coalesce into a smooth film. The increase in surface coverage of these smooth films was offset somewhat by a decrease for each particle of the area exposed to the electrolyte, so the catalytic activity increased only slightly, to a plateau, after a few s of deposition.

In contrast, when deposited for long periods of time, Ni–Mo did not produce coalescing, smooth films. Instead, Ni–Mo deposited in a multilayer structure that had a high surface roughness, which resulted from the small crystallite size of the deposits. The activity toward the HER for Ni–Mo films on Si therefore increased monotonically, up to rather long total deposition times. The Ni–Mo deposits thus provided relatively higher activity than pure Ni, likely due to a combination of slightly higher fundamental activity and substantially enhanced surface area.

Pt films that were produced by electroless deposition exhibited the highest activity after 4–6 min of deposition from a 1 mM Pt (IV) salt solution. The resulting morphology was a nano-particulate network similar to that produced by the short-time deposition of Ni–Mo or Ni. However, the catalytic behavior of electroless Pt on planar p⁺-Si at >10 mA cm⁻² was dominated by a large series resistance. This resistance was likely due to the formation of a barrier layer between the Si surface and the Pt nanoparticles.

A mechanism for the electroless deposition of Pt on Si involves the sacrificial oxidation of surface Si, and subsequent removal by HF [eqn (11) and (12)].[21]

$$H_2PtCl_6 + Si^0 + 2H_2O \rightarrow Pt^0 + SiO_2 + 6HCl \qquad (11)$$

$$SiO_2 + 6HF \rightarrow H_2SiF_6 + 2H_2O \qquad (12)$$

Some oxidized Si sites may not be accessible to etching by HF, due to the presence of the Pt overlayer. As a result, the interfacial region between the Si and the electrolessly deposited Pt nano-particles could have an insulating Si oxide, yielding the observed

resistive behavior of the electrodes. This hypothesis is consistent with the observations that (a) e-beam evaporated Pt exhibited no such resistive behavior, presumably because this deposition process did not involve the chemical oxidation of Si, and (b) electroless Pt deposits on Si microwires did not show such pronounced resistive behavior, because the greater surface roughness would provide many more parallel paths by which electrons might traverse the interface, resulting in a lower overall resistance of the catalyst-coated electrode.

XPS analysis was performed to elucidate the state of the Si surface under various conditions of Pt deposition (Fig. 9). A planar p⁺-Si sample coated with electroless Pt, from a 1 mM Pt (IV)/HF(aq) solution, showed markedly higher levels of oxidized Si than a bare Si control, or than a sample that had been coated with a deposit of e-beam evaporated Pt. These data strongly support the formation of an interfacial oxide on Si in the presence of Pt(IV) salts, which is consistent with the resistive behavior observed in the HER experiments.

The observed activity of a given electrocatalyst was higher on p⁺-Si microwire arrays than on planar p⁺-Si. These higher observed activities are consistent with the increased total amount of catalyst that resulted from microstructuring of the wire array electrode. Electron microscopy also indicated that the catalyst conformally coated the entire length of the p⁺-Si microwires. The increase in observed activities for the Ni and Ni–Mo deposits on the Si microwire arrays was comparable to the surface roughness factor $\gamma \sim 6$ of the particular Si microwire array electrodes used in this study. These observations indicate that the micro-structured geometry effected a significant enhancement in the observed electrocatalytic activity. This enhancement is in addition to that provided from nanostructuring of the electro-deposited catalysts themselves, suggesting that roughness effects on the micro- and nano-scale are multiplicative (i.e. $\gamma_{total} = \gamma_{nano} \cdot \gamma_{micro}$). The observations also indicate a relatively facile
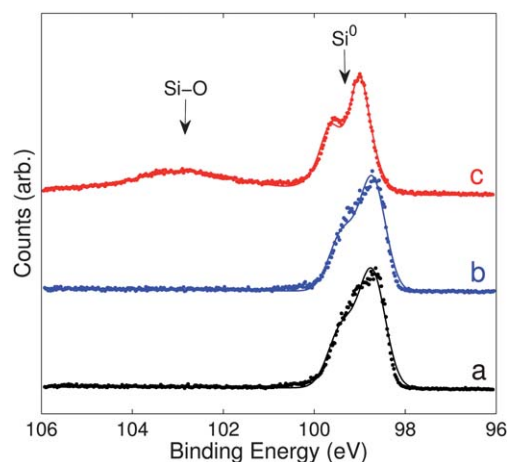

Fig. 9 XP spectra of the Si 2p region of three p⁺-Si samples: (a) control sample with no deposition; (b) coated with Pt *via* e-beam evaporation; (c) coated with Pt *via* electroless deposition. In all three cases, samples were treated in nominally the same fashion, other than the deposition conditions, and were freshly etched in buffered HF(aq) immediately before introduction into the analysis chamber. Sample (c) showed significant surface oxidation, while samples (a) and (b) showed little to no detectable signals attributable to oxidized Si.

mass transport of reactant and product species to and from the base of the microwires. The performance of the Ni–Mo catalyst on p⁺-Si microwires approached the activity of e-beam evaporated Pt films on planar Si, which has been shown to possess sufficient catalytic activity to enable highly efficient hydrogen production on Si p–n⁺ junction photoelectrodes.[12] This remarkably high activity for a non-noble catalyst likely results from the aforementioned increase in surface area along with a relatively smaller enhancement due to alloying Ni with Mo. Previous work suggests the fundamental catalytic activity of bulk Ni–Mo alloy is relatively insensitive to the concentration of Mo,[32] and the fundamental (*i.e.* surface area normalized) activity for our coatings is being evaluated in detail at present.

D. Photoelectrode/catalyst systems

Despite the higher catalytic activity of Ni–Mo relative to Ni, planar p-Si photoelectrodes coated with Ni or Ni–Mo showed mutually similar overall, thermodynamically based, efficiencies for the conversion of incoming simulated sunlight to $H_2(g)$. This behavior primarily resulted from the lower photovoltages exhibited by p-Si electrodes coated with Ni–Mo relative to p-Si photoelectrodes coated with Ni.

The difference in photovoltage between Ni and Ni–Mo coated Si photocathodes is consistent with the behavior expected from inherent differences in the energetics of the mixed Si-catalyst and Si-electrolyte interfaces. Both nanostructured systems are expected to operate in the regime of the "pinch-off" effect, in which the photovoltage generated by the p-Si/catalyst/electrolyte system of an appropriate geometry is dominated by the energetics of the interfacial region that has the larger barrier between the p-Si and the contacting phase.[36,37] The geometry in which this effect is most beneficial (*i.e.* yielding the highest V_{oc}) is one in which the metal particles are widely separated from one another and have small areas of contact with the Si. Based on images collected from electron microscopy, the Ni–Mo nanoparticles were individually smaller, but made more extensive contact and were closer together on the Si surface, than the Ni nanoparticles. Hence, the Ni–Mo catalyst coating was likely to be less "pinched off," consistent with the lower photovoltages observed for Ni–Mo relative to Ni deposits.

The similarity in efficiencies for light-driven $H_2(g)$ evolution between p-Si/Ni and p-Si/Ni–Mo electrodes illustrates that an increased surface area of the catalyst film does not necessarily result in enhanced performance of photoelectrodes. A higher catalyst loading increases the turnover rates for a given electrode area, but also significantly influences other parameters of the system, including the interfacial energetics and the absorption of light by the semiconductor.

Pt films on p-Si exhibited perhaps the most interesting behavior of any of the three tested electrocatalyst materials. Electroless Pt deposition resulted in an interfacial oxide, which inhibited electron transport through the catalyst, enabling the pinch-off condition in which the Si/electrolyte barrier dominated the photovoltage. Conversely, e-beam evaporated Pt, with no interfacial barrier, produced sufficiently facile electron transfer through Si-Pt-electrolyte that the interfacial energetics were dominated by the ohmic contact to Pt, resulting in no photovoltage. An implication of this observed behavior is that Pt may

not, in fact, be an appropriate material to couple directly with Si photocathodes for efficient H_2 evolution, as it forces a tradeoff between high catalytic activity (clean interface) and high photovoltage (barrier layer). Additional characterization of the Si/Pt interface, with strict control over catalyst geometry and morphology, would thus be a useful addition to the understanding of this system.

Microwire array p-Si photoelectrodes showed similar behavior to planar p-Si photoelectrodes, except that the catalytic activity was higher, and the photocurrent densities were markedly lower for the microwire array electrodes relative to the planar electrodes. The difference in observed photocurrent density is consistent with the lower photon flux absorbed by the as-prepared microwire array electrodes. Studies of light absorption have revealed the origin of the lower photocurrents in Si microwire arrays than in planar Si samples, and have demonstrated how incorporating light scattering/randomizing elements into the wire array structures can mitigate these effects.[38] Additionally, enhanced control over the interfacial energetics of the p-Si/catalyst/electrolyte system, including identification and elimination of deleterious surficial and/or interfacial electronic states, would be beneficial to attain yet higher photovoltages than those reported herein and thus to obtain corresponding increases in the efficiency of conversion of incident optical energy into $H_2(g)$.

V. Conclusions

Ni, Ni–Mo, and Pt catalysts have been deposited onto p-type and degenerately doped p⁺-Si substrates in planar and microwire geometries. The two non-noble catalysts were both sufficiently active on p-type Si to give a net storage of incoming photon energy in the form of $H_2(g)$. Deposition of these catalysts onto Si microwire arrays enhanced the apparent activities due to increases in surface area. Ni–Mo alloy showed sufficient catalytic activity on the microwire arrays to make it a promising non-noble alternative to Pt, but the photocurrents and photovoltages generated by as-grown p-Si microwire electrodes are insufficient to allow optimal net energy storage. Thus, if methods can be devised to increase the photovoltage generated by illuminated p-Si $H_2(g)$ evolving microwire photocathodes, Ni–Mo would be an attractive alternative to noble metals for semiconductor-coupled $H_2(g)$ evolution from sunlight.

Acknowledgements

Notes and references

1 N. S. Lewis and D. G. Nocera, *Proc. Natl. Acad. Sci. U. S. A.*, 2006, **103**, 15729–15735.

2 N. Lewis, G. Crabtree, A. Nozik, M. Wasielewski and P. Alivisatos, *DOE BES report on basic energy sciences workshop: Basic research needs for solar energy utilization*, 2005, http://www.er.doe.gov/bes/reports/abstracts.html#SEU.

3 M. Walter, E. Warren, J. McKone, S. Boettcher, M. Qixi, L. Santori and N. Lewis, *Chem. Rev.*, 2010, **110**, 6446–6473.

4 A. Heller and R. G. Vadimsky, *Phys. Rev. Lett.*, 1981, **46**, 1153–1156.

5 R. N. Dominey, N. S. Lewis, J. A. Bruce, D. C. Bookbinder and M. S. Wrighton, *J. Am. Chem. Soc.*, 1982, **104**, 467–482.

6 R. E. Rocheleau, E. L. Miller and A. Misra, *Energy Fuels*, 1998, **12**, 3–10.

7 O. Khaselev and J. A. Turner, *Science*, 1998, **280**, 425–427.

8 B. M. Kayes, H. A. Atwater and N. S. Lewis, *J. Appl. Phys.*, 2005, **97**, 114302.

9 B. M. Kayes, M. A. Filler, M. C. Putnam, M. D. Kelzenberg, N. S. Lewis and H. A. Atwater, *Appl. Phys. Lett.*, 2007, **91**, 103110.

10 J. M. Spurgeon, K. E. Plass, B. M. Kayes, B. S. Brunschwig, H. A. Atwater and N. S. Lewis, *Appl. Phys. Lett.*, 2008, **93**, 032112.

11 M. C. Putnam, S. W. Boettcher, M. D. Kelzenberg, D. B. Turner-Evans, J. M. Spurgeon, E. L. Warren, R. M. Briggs, N. S. Lewis and H. A. Atwater, *Energy Environ. Sci.*, 2010, **3**, 1037–1041.

12 S. W. Boettcher, E. L. Warren, M. C. Putnam, E. L. Santori, D. Turner-Evans, M. D. Kelzenberg, M. G. Walter, J. R. McKone, B. S. Brunschwig, H. A. Atwater and N. S. Lewis, *J. Am. Chem. Soc.*, 2010, **133**, 1216–1219.

13 S. Trasatti, in *Advances in Electrochemical Science and Engineering*, ed. H. Gerischer and C. Tobias, VCH, Weinheim, Germany, 1992, vol. 2, ch. 1, pp. 1–85.

14 S. Trasatti, *J. Electroanal. Chem.*, 1972, **39**, 163–184.

15 M. Miles, *J. Electroanal. Chem.*, 1975, **60**, 89–96.

16 J. Divisek, H. Schmitz and J. Balej, *J. Appl. Electrochem.*, 1989, **19**, 519–530.

17 J. Jaksic, M. Vojnovic and N. Krstajic, *Electrochim. Acta*, 2000, **45**, 4151–4158.

18 I. Raj, *J. Mater. Sci.*, 1993, **28**, 4375–4382.

19 J. G. Highfield, E. Claude and K. Oguro, *Electrochim. Acta*, 1999, **44**, 2805–2814.

20 Y. Tsuru, M. Nomura and F. Foulkes, *J. Appl. Electrochem.*, 2002, **32**, 629–634.

21 I. Lombardi, S. Marchionna, G. Zangari and S. Pizzini, *Langmuir*, 2007, **23**, 12413–12420.

22 For the purposes of this report, the current density is the ratio of the current passed to the macroscopic (also called geometric or projected) area of the sample.

23 S. Trasatti and O. Petrii, *J. Electroanal. Chem.*, 1992, **327**, 353–376.

24 B. Conway, H. Angerstein-Kozlowska, M. Sattar and B. Tilak, *J. Electrochem. Soc.*, 1983, **130**, 1825–1836.

25 S. W. Boettcher, J. M. Spurgeon, M. C. Putnam, E. L. Warren, D. B. Turner-Evans, M. D. Kelzenberg, J. R. Maiolo, H. A. Atwater and N. S. Lewis, *Science*, 2010, **327**, 185–187.

26 J. Stachurski, D. Pouli, J. Ripa and G. Pokrzyk, *Low overvoltage hydrogen cathodes*, U.S. Patent 4,354,915, 1982.

27 I. Raj and V. Venkatesan, *Int. J. Hydrogen Energy*, 1988, **13**, 215–223.

28 C. Fan, D. Piron, A. Sleb and P. Paradis, *J. Electrochem. Soc.*, 1994, **141**, 382–387.

29 D.-L. Long, E. Burkholder and L. Cronin, *Chem. Soc. Rev.*, 2007, **36**, 105–121.

30 A. Müller and C. Serain, *Acc. Chem. Res.*, 2000, **33**, 2–10.

31 E. Chassaing, K. Quang and R. Wiart, *J. Appl. Electrochem.*, 1989, **19**, 839–843.

32 M. de Chialvo and A. Chialvo, *J. Electroanal. Chem.*, 1998, **448**, 87–93.

33 J. O. M. Bockris, I. A. Ammar and A. K. M. S. Huq, *J. Phys. Chem.*, 1957, **61**, 879–886.

34 D. Brown, M. Mahmood, A. Turner, S. Hall and P. Fogarty, *Int. J. Hydrogen Energy*, 1982, **7**, 405–410.

35 D. Brown, M. Mahmood, M. Man and A. Turner, *Electrochim. Acta*, 1984, **29**, 1551–1556.

36 J. Freeouf, T. Jackson, S. Laux and J. Woodall, *J. Vac. Sci. Technol.*, 1982, **21**, 570–573.

37 R. C. Rossi and N. S. Lewis, *J. Phys. Chem. B*, 2001, **105**, 12303–12318.

38 M. D. Kelzenberg, S. W. Boettcher, J. A. Petykiewicz, D. B. Turner-Evans, M. C. Putnam, E. L. Warren, J. M. Spurgeon, R. M. Briggs, N. S. Lewis and H. A. Atwater, *Nat. Mater.*, 2010, **9**, 239–244.